ELSEVIER

Contents lists available at ScienceDirect

### Materials Science & Engineering A

journal homepage: www.elsevier.com/locate/msea





## Enhanced mechanical properties of Ti-5Al-5Mo-5V-3Cr-1Zr by bimodal lamellar precipitate microstructures via two-step aging

Yalong Wang <sup>a,e</sup>, Mengyuan Hao <sup>a</sup>, Dian Li <sup>b</sup>, Pei Li <sup>a,d</sup>, Qianglong Liang <sup>a</sup>, Dong Wang <sup>a,\*</sup>, Yufeng Zheng <sup>b,\*\*</sup>, Qiaoyan Sun <sup>a,\*\*\*</sup>, Yunzhi Wang <sup>c</sup>

- <sup>a</sup> Center of Microstructure Science, Frontier Institute of Science and Technology, State Key Laboratory for Mechanical Behavior of Materials, Xi'an Jiaotong University, Xi'an. 710049. China
- <sup>b</sup> Department of Chemical and Materials Engineering, University of Nevada Reno, 1664N. Virginia St., Reno, NV, 89557, USA
- <sup>c</sup> Department of Material Science and Engineering, Center for the Accelerated Maturation of Materials (CAMM), The Ohio State University, 2041 College Rd., Columbus, OH, 43210, USA
- d Thermal Power Research Institute Co. Ltd., Xi'an, 710032, PR China
- <sup>e</sup> Lanzhou Institute of Physics, Lanzhou, Chengguan District, Feiyan Street No. 100, China

#### ARTICLE INFO

# $\begin{tabular}{ll} \textit{Keywords:} \\ \textbf{Titanium alloys} \\ \alpha \ precipitation \\ \textbf{Pseudo-spinodal decomposition} \\ \textbf{Mechanical properties} \\ \end{tabular}$

#### ABSTRACT

The formation of ultra-fine  $\alpha$  precipitates in  $\beta$ -titanium alloys can significantly improve strength but may lead to rupture and low ductility. Here, we propose a simple two-step aging heat treatment to design a bimodal microstructure with distinctively different populations of fine-scale and coarse  $\alpha$  precipitates in Ti-5Al-5Mo-5V-3Cr-1Zr (Ti-55531, wt. %) by involving two transformation mechanisms, i.e., classical nucleation and growth, and pseudo-spinodal decomposition. Such a multi-scale  $\alpha$  microstructure exhibits a synergistic combination of yield strength (~1.1 GPa) and ductility (~19.5% elongation). TEM characterization shows that the appearance of deformation twins in coarse  $\alpha$  precipitates contribute to increased ductility, and the higher strength may be attributed to dislocation tangles in fine-scale  $\alpha$  precipitates. Our work provides a new strategy to overcome the strength-ductility trade-off by designing a heterogeneous microstructure.

#### 1. Introduction

Titanium alloys (Ti-alloys) have broad applications in aerospace, automobile, medical and sport industries [1] due to their high specific strength, good corrosion resistance, and excellent bio-compatibility [2–5]. However, many new applications demand further improving the comprehensive mechanical properties of Ti-alloys, which requires overcoming the strength-ductility trade-off [6]. Systematic investigations on typical high-strength Ti-alloys, e.g., Ti-5Al-5Mo-5V-3Cr (Ti-5553, wt. %) and Ti-5Al-5Mo-5V-3Cr-1Zr (Ti-55531, wt. %), demonstrate that the improvement of strength is accompanied by the deterioration of ductility [7–9]. For example, bimodal and lamellar  $\alpha$  microstructures have been developed in these Ti-alloys [10–12]. It is reported that the lamellar microstructure (LM) of Ti-5553 has shown a high ultimate tensile strength (UTS) (1.2 GPa) but a relatively low ductility (~5.5% elongation) [11]; on the other hand, a bimodal

microstructure (BM) possesses a low UTS (1.1 GPa) but an improved ductility (13.4% elongation) [10]. The LM in Ti-55531 exhibits a relatively high UTS (1.2 GPa) with a large total elongation (10.5%), and the BM with finer secondary  $\alpha$  shows a combination of high UTS (1.3 GPa) and low ductility (8.5%) [12]. Existing data from literature [7,9–13] as plotted in Fig. 1(a) indicate that the currently available Ti-alloys have not been able to break out the strength-ductility trade-off.

Recent studies have shown that alloys with heterogeneous grain microstructures (e.g., a mixture of grains having micrometer and nanometer sizes [14,15]) could exhibit a synergistic combination of strength and ductility. Since most engineering alloys are strengthened by second-phase precipitates, we explore the possibility in achieving such a synergistic combination by designing heterogeneous precipitate microstructures in Ti-alloys. It is known that the strength of Ti-alloys can be improved by increasing the volume fraction of  $\alpha$  phase and refining the size of  $\alpha$  precipitates, while improving the ductility requires the

E-mail addresses: wang\_dong1223@mail.xjtu.edu.cn (D. Wang), yufengz@unr.edu (Y. Zheng), qysun@mail.xjtu.edu.cn (Q. Sun).

<sup>\*</sup> Corresponding author.

<sup>\*\*</sup> Corresponding author.

<sup>\*\*\*</sup> Corresponding author.

opposites [16,17]. The size, shape, and density of  $\alpha$  precipitates can be tuned through three different phase transformation mechanisms [18–20]: (a) unimodal coarse  $\alpha$  precipitates with low strength but high ductility [19,21] can be obtained via the classical nucleation and growth mechanism by aging at relatively high temperatures in the  $\alpha+\beta$  two-phase region; (b) fine-scale  $\alpha$  precipitates with intermediate strength and ductility can be obtained via the pseudo-spinodal decomposition mechanism by aging at a specific temperature range in the  $\alpha+\beta$  two-phase region [18,22]; (c) super-refine  $\alpha$  precipitates with high strength and low ductility can be obtained via isothermal  $\omega$  assisted nucleation mechanism by slowly heating + aging [8,20]. Thus, we hypothesize that if a heterogeneous  $\alpha$  precipitate microstructure as the one shown schematically in Fig. 1(b) III could be achieved in Ti-alloys, improved mechanical properties including both high strength and high ductility may be realized.

Driven by this hypothesis and guided by recent studies on non-conventional phase transformation pathways present in Ti-alloys [23, 24], we design a two-step aging heat treatment (i.e., aging at 700 °C/3h followed by aging at 600 °C/3h in Fig. 1(c)) to achieve such a heterogeneous  $\alpha$  precipitate microstructure in Ti-55531. This two-step heat treatment avoids the formation of brittle  $\omega$  phase at low temperatures and generates lamellar  $\alpha$  precipitates in two distinctively different sizes. Tensile tests show that the alloy has a combination of a UTS of  $\sim\!1.1$  GPa and a ductility of  $\sim\!19.5\%$  total elongation, as shown by the red star symbol in Fig. 1(a).

#### 2. Methods

#### 2.1. Experimental procedures

Ti-55531 (Ti-5.2Al-4.79Mo-4.83V-2.77Cr-1.07Zr-0.35Fe, wt. %) was prepared by electric arc melting. The  $\beta$ -transus temperature of the alloy, determined by the metallographic method, is  $(835 \pm 5)^{\circ}$ C. Disc samples in 10 mm thickness were  $\beta$ -solutionized at 850 °C for 60 min before subsequent aging. For the two-step aging, the  $\beta$ -solution samples were down-quenched to 700  $^{\circ}$ C, isothermally held for 180 min, and followed by down-quenching to 600  $^{\circ}\text{C}$  for isothermal holding for 180 min, and finally, water-quenched (WQ) to room temperature (See Fig. 1(c)). To compare, a single-step aging heat treatment was also carried out, where the β-solutionized samples were either aged at 700 °C for 180 min followed by WQ or aged at 600 °C for 180 min followed by WQ. All aged samples were etched in a solution of V (HF): V (HNO3): V (H2O) = 2%: 8%: 90%. The microstructure of heat-treated samples was then characterized using SU-6600 scanning electron microscope (SEM) at 15 kV and JEOL JEM-2100F transmission electron microscope (TEM) at 200 kV. SEM images were further processed and quantitatively analyzed using MIPAR<sup>TM</sup> image processing software. In addition, tensile tests of all the aged samples were carried out at room temperature with a sample size of 6 mm in diameter and 30 mm in gauge distance at a strain rate of 5.6  $\times$ 10<sup>-4</sup>·s<sup>-1</sup> using the INSTRON 1195 universal testing system.

#### 2.2. Phase field model

A set of conserved field (c) and nonconserved field ( $\eta$ ) variables is

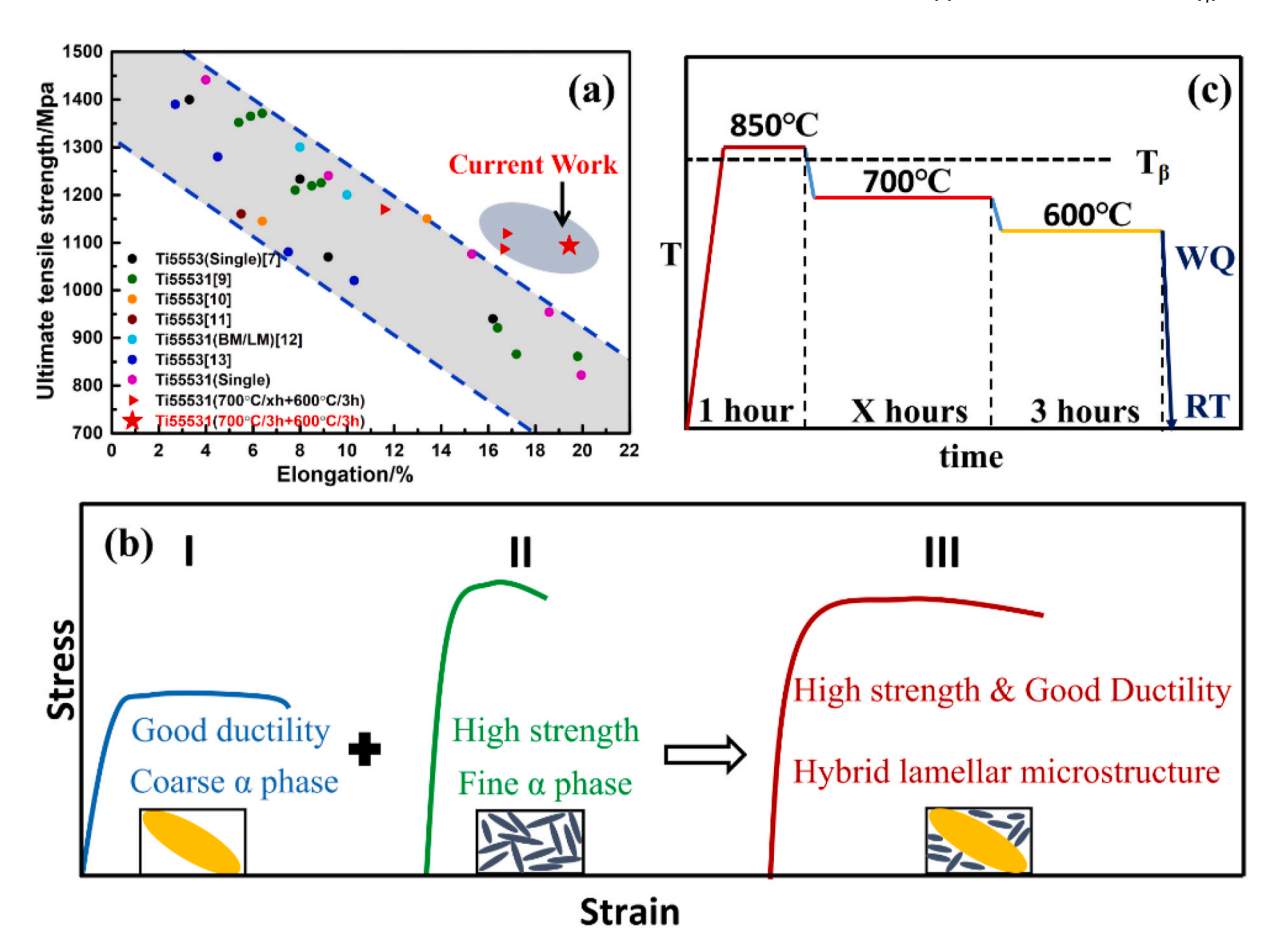


Fig. 1. (a) Ultimate tensile strength and total elongation relationship for Ti5553 (black, orange, wine, and blue dots) and Ti55531 (cyan and dark green dots) from the literature [7,9-13] and current work (pink dots for single-step aging, red triangle, and star for two-step aging); (b) Schematic drawing for the design of heterogeneous lamellar microstructure consisting of coarse and fine  $\alpha$  precipitates; (c) The two-step aging heat treatment schedule used in the current work. (For interpretation of the references to color in this figure legend, the reader is referred to the Web version of this article.)

used to describe the total free energy expression of a binary system (Ti-Mo) as follow [25].

the related mechanical properties (UTS and maximum strain). The alloy from 600  $^{\circ}$ C/3h single-step aging exhibits a higher strength (UTS  $\sim$ 1.2

$$F = \int_{V} \left[ \sum_{P} h(\eta_{P}) g_{a}(c_{Mo}, T) + \left( 1 - \sum_{P} h(\eta_{P}) \right) g_{\beta}(c_{Mo}, T) + \omega_{1} \sum_{P} \sum_{P \neq q} \eta_{P} \eta_{q} + \sum_{P} \omega_{2} \left( \eta_{P}^{2} - 2 \eta_{P}^{3} + \eta_{P}^{4} \right) + \frac{\kappa}{2} (\nabla c_{Mo})^{2} + \frac{\lambda}{2} \sum_{P} (\nabla \eta_{P})^{2} + E^{elastic} \right]$$

$$(1)$$

where  $c_{Mo}$  is the concentration field,  $\eta_i$  is the structure field of the ith  $\alpha$ variants.  $w_1$  and  $w_2$  stand for the hump height of the free energy surface between  $\beta$  and  $\alpha$  phases and among different alpha variants.  $\kappa$  and  $\lambda$  are the gradient energy coefficients for concentration and structural field, respectively.  $h(\eta_i)$  is an interpolation function  $h(\eta) = \eta^3 (6\eta^2 - 15\eta +$ 10). The elastic energy is given by the Khachaturyan-Shatalov theory,  $E^{elastic} = \frac{1}{2} \int_{V} \frac{d\overrightarrow{k}}{2\pi^3} \sum_{p,q}^{3} B_{pq}(\overrightarrow{n}) \widetilde{\eta}_p(\overrightarrow{k}) \widetilde{\eta}_q^*(\overrightarrow{k})$  [26].  $B_{pq}(\overrightarrow{n})$  stands for a function of the transformation strains of each  $\alpha$  variant,  $B_{pq}(\overrightarrow{n}) =$  $C_{ijkl} \varepsilon_{kl}^T(p) \varepsilon_{kl}^T(q) - \overrightarrow{n}_i \sigma_{ii}^T(p) \Omega_{ik}(\overrightarrow{n}) \sigma_{kl}^T(q) \overrightarrow{n}_l$ , where  $C_{ijkl}$  represents the stiffness tensor, and  $\varepsilon_{ii}^T(p)$  stands for the stress-free transformation strain of the pth variant,  $\sigma_{ij}^T(p) = C_{ijkl} \varepsilon_{kl}^T$ ,  $[\Omega(\overrightarrow{n})]_{ik}^{-1} = C_{ijkl} n_j n_l$ . The value of stress-free transformation strain can be derived from the Burgers orientation relationship and symmetry operations. According to the calculated free energy, the evolution of concentration diffusion and structure transformation in phase field model can be obtained by solving Chan-Hilliard (CH) equation  $\frac{\partial c_{Mo}}{\partial t} = \nabla \left[ M \nabla \frac{\delta F}{\delta c_{Mo}} \right] + \xi_c$  as well as Ginzburg-Landau (TDGL) equation  $\frac{\partial \eta_p}{\partial t} = -L \frac{\delta F}{\delta \eta_p} + \xi_{\eta}$ , respectively, where Mstands for the chemical mobility of Mo, and L stands for the structural mobility of the  $\eta$ , and  $\xi_c$  and  $\xi_n$  are the Langevin force terms to simulate nucleation.

#### 3. Results

#### 3.1. Mechanical properties

Fig. 2 shows the engineering stress-strain curves of all aged samples along with those  $\beta\text{-}solutionized$  without aging, and the inset table shows

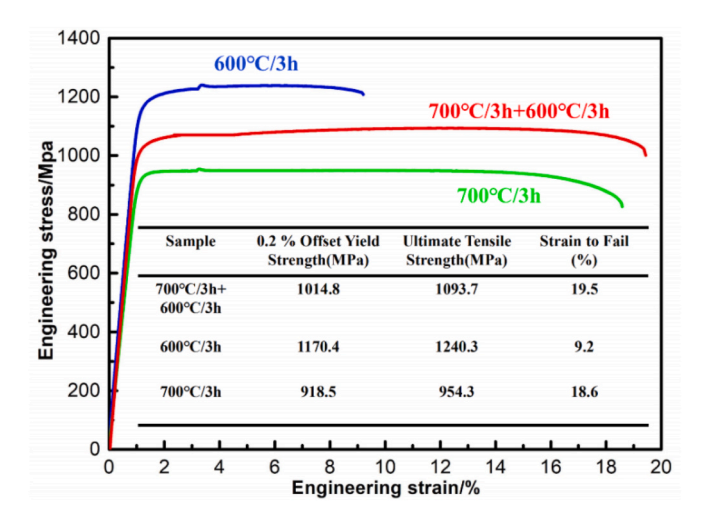


**Fig. 2.** Engineering stress-strain curves at room temperature for samples after 600  $^{\circ}$ C single-step aging, 700  $^{\circ}$ C + 600  $^{\circ}$ C two-step aging, and 700  $^{\circ}$ C single step-aging, respectively. The inset table describes the related mechanical properties of Ti-55531 under different heat treatments.

GPa) but a lower ductility (~9.2% total elongation) as compared to the alloy from 700 °C/3h single-step aging (UTS ~0.9 GPa and total elongation ~18.6%). This describes a typical strength-ductility trade-off in Ti-alloys. The increase of strength always accompanies the decrease of ductility. In contrast, the alloy after 700 °C/3h + 600 °C/3h two-step aging shows a combination of intermediate strength (~1.1 GPa) and high ductility (~19.5% total elongation). Although the two-step aged alloy has a lower strength than that of the 600 °C single-step aged alloy, its total strain to failure is significantly larger. The results demonstrate that Ti-55531 from the two-step aging has a superior combination of strength and ductility, as indicated by the red star in Fig. 1(a).

#### 3.2. Microstructural characteristics

The microstructures of different Ti-55531 samples from different heat treatments are shown in Fig. 3. The sample after  $\beta$ -solution treatment has shown a single  $\beta$  phase with an average grain size of  $\sim 100 \ \mu m$ (Fig. 2 (a) and (e)). The choice of relatively low temperature (only 25 °C higher than  $T_β$ ) for β-solutionizing is to limit β grain growth. No α phase has been observed after solution treatments. Fig. 3(b) and (f) show the microstructure of a sample single-step aged at 700 °C. Coarse  $\alpha$  laths can be observed, with an average length of  ${\sim}6.93\pm2.16~\mu m$  and width of  $\sim$ 0.81  $\pm$  0.32  $\mu$ m. Most of these laths are close to grain boundaries and some are formed in grain interior. Fig. 3(c) and (g) show the microstructure of a sample single-step aged at 600  $^{\circ}$ C, in which fine-scale  $\alpha$ laths (average length of  $\sim$  3.7  $\pm$  1.4  $\mu m$  and width  $\sim$  0.2  $\pm$  0.04  $\mu m$ ) with uniform spatial distribution can be found. The formation of homogeneous fine-scale  $\alpha$  laths with high number density at low aging temperature (600 °C) could be attributed to the pseudo-spinodal decomposition mechanism [18], while coarse  $\alpha$  laths with low number density at higher aging temperature (700 °C) are believed to form via the classical nucleation and growth mechanism [19,22]. Fig. 3(d) and (h) show the microstructure of a sample two-step aged, which exhibits a bimodal size distribution with fine  $\alpha$  laths (an average length  $\sim$ 1.66  $\pm$ 0.5  $\mu m$  and width  $\sim 0.15 \pm 0.06 \ \mu m$ ) and coarse  $\alpha$  laths (an average length  $\sim$ 7.11  $\pm$  2.29  $\mu m$  and width  $\sim$ 0.78  $\pm$  0.26  $\mu m$ ).

Fig. 3 (i) (k) and (l) show the quantitative analyses of the corresponding SEM images processed by MIPAR<sup>TM</sup> software application. The results indicate that the area fractions of  $\alpha$  precipitates in the different samples are approximately 30%, 50.2%, and 46.3% respectively, and the number densities of  $\alpha$  precipitates are 0.14 laths/ $\mu$ m<sup>2</sup>, 2.77 laths/ $\mu$ m<sup>2</sup>, and 1.89 laths/ $\mu$ m<sup>2</sup>, respectively. Overall, these SEM images confirm that the two-step aging successfully introduced a mixture of fine and coarse  $\alpha$  precipitates Ti-55531 with high volume fraction, which is responsible for the improved mechanical properties in Fig. 2.

To analyze the microstructure of heterogeneous  $\alpha$  precipitates after two-step aging, Fig. 4 shows the size distribution of different microstructures. Uniform microstructure (UM) describes a homogeneous distribution of fine  $\alpha$  precipitates after single-step aging at 600 °C/3h and 700 °C/3h, and heterogeneous microstructure (HM) is corresponding to a bimodal distribution of  $\alpha$  precipitates after two-step aging at 700 °C/3h + 600 °C/3h. HM has shown two peaks representing different sizes (7  $\mu m$  and 1.0  $\mu m$ ) of  $\alpha$  precipitates. Interestingly, UM has shown a single peak representing a similar size (1.6  $\mu m$ ) of  $\alpha$  precipitates after aging at 600 °C/3h, which is larger than that of HM. In addition,

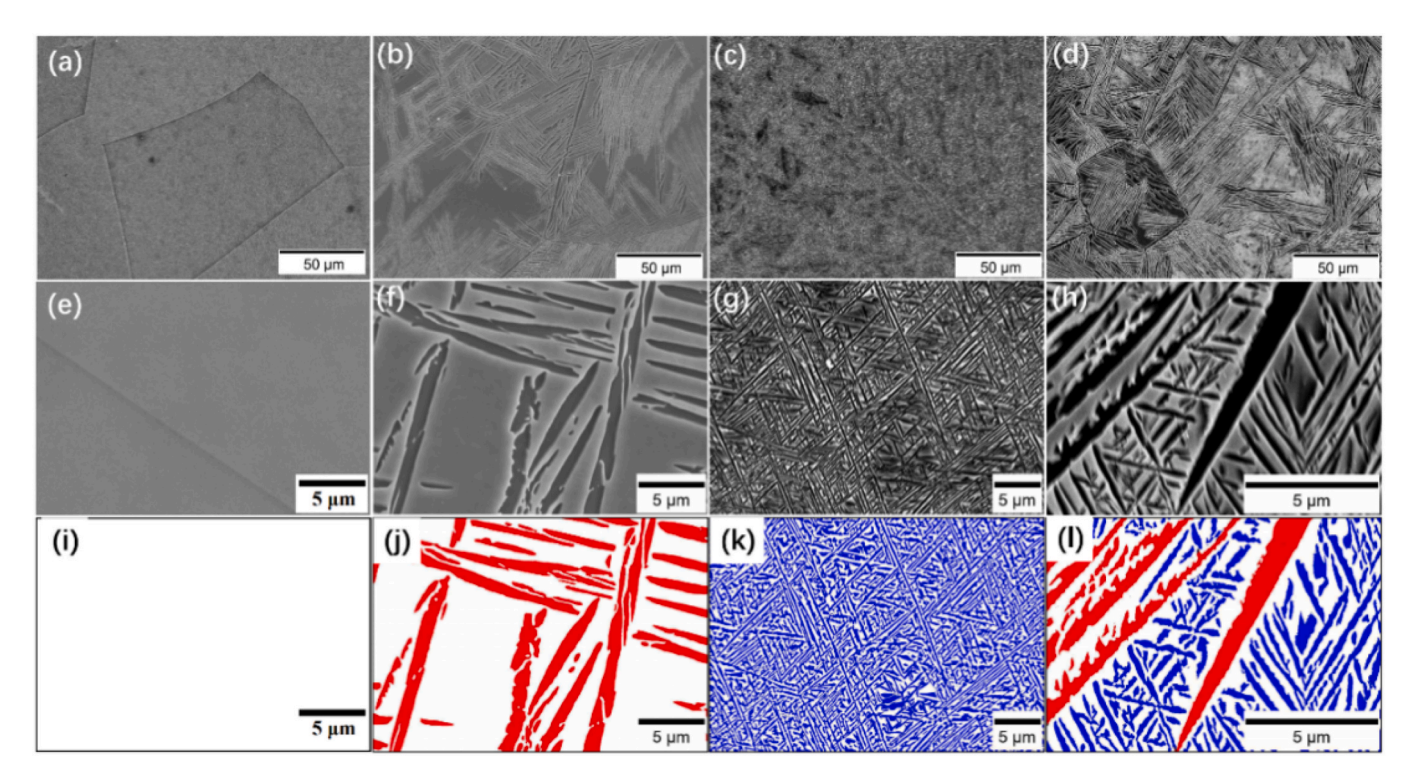


Fig. 3. Microstructures of Ti-55531 samples after different heat treatments and then water quenched to room temperature. (a) and (e) The SEM images after solution treatment at 850 °C for 1h, (b) and (f) followed by aging at 700 °C for 3h, (c) and (g) followed by aging at 600 °C for 3h, and (d) and (h) followed by two-step aging at 700 °C for 3h and 600 °C for 3h. (i)–(l) Quantitative image analyses of the corresponding SEM images by MIPAR<sup>TM</sup>, with the red color representing coarse  $\alpha$  and blue color representing fine  $\alpha$  precipitates. (For interpretation of the references to color in this figure legend, the reader is referred to the Web version of this article.)

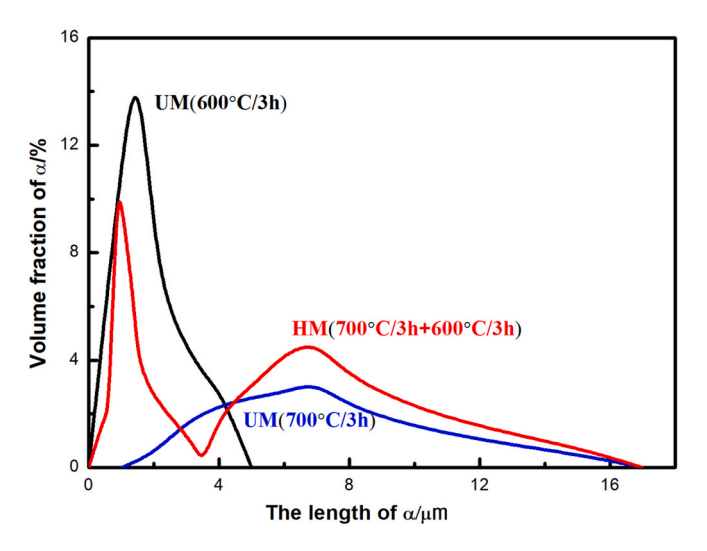


Fig. 4. Size distribution of  $\alpha$  precipitates for Ti55531 alloys with different heat treatments. UM represents the uniform microstructure with a homogeneous distribution of  $\alpha$  precipitates after single-step aging at 600 °C/3h and 700 °C/3h respectively, HM represents the heterogeneous microstructure with different size of  $\alpha$  precipitates after two-step aging at 700 °C/3h + 600 °C/3h.

coarse  $\alpha$  precipitates after first aging (700 °C/3h) grow with the increase of volume fraction after 2nd aging (600 °C/3h).

#### 3.3. Deformation mechanism

To understand the deformation behaviors of the two-step aged sample, TEM characterization of the deformation microstructure was carried out after the tensile test and the results are shown in Fig. 5. The selected plastic deformation zone of the tensile specimen is shown by the

dashed red line in Fig. 5(a), which is close to the region of fracture ( $\sim$ 19.5% deformation). Fig. 5(b) shows the related bright field image of the fine  $\alpha$  region and the inset shows the diffraction pattern, where no deformation twins can be observed in these regions. There may exist lots of dislocation tangles in both  $\beta$  and  $\alpha$  phase as labeled by white color in Fig. 5(b). Different from the deformation mechanism of fine  $\alpha$  precipitates, Fig. 5(c) shows the appearance of deformation twin in coarse  $\alpha$  region as labeled by red dash lines. Fig. 5(d) exhibits the corresponding diffraction pattern from the white circle region in Fig. 5(c), which confirms the deformation twin structure. There also exist dislocations inside the coarse  $\alpha$  laths and  $\beta$  matrix.

There exist three different types of twinning systems in  $\alpha\textsc{-Ti}$ : twinning of  $\{10\overline{1}2\}$  and  $\{11\overline{2}1\}$  types are expected in extension along  $\langle c \rangle$  axis,  $\{11\overline{2}2\}$  and  $\{10\overline{1}1\}$  types are expected in compression along  $\langle c \rangle$  axis, depending on the grain orientation [27]. At low deformation (10%),  $\{11\overline{2}2\}$  compression twin was dominant, the  $\{10\overline{1}2\}$  tension twin was increased with the increase of deformation (20%). However, the orientations of  $\alpha$  and  $\beta$  phases in  $\beta\textsc{-Ti}$  alloys (our current systems) obey the Burger's orientation relationship, which could induce inter-phase interaction during plastic deformation and influence the deformation behavior of  $\beta\textsc{-Ti}$  alloys. It was reported that  $\alpha$  precipitates take much less elastic strain than the  $\beta$  matrix in  $\beta\textsc{-Ti}$  alloys, and the stress redistribution between  $\alpha$  precipitates and  $\beta$  matrix occurred to accommodate the inter-phase interaction [28].

The  $\alpha/\beta$  interfaces act as potential sites for the evolution of dislocations, dislocation pile-up. Dislocations in  $\beta$  matrix get obstructed at  $\alpha/\beta$  interface and form pile up at these interfaces under loading, which provides higher local stress on the  $\alpha$  phase. Certain easy slip transfer into some favorably oriented  $\alpha$  precipitates and form dislocation tangling. Other  $\alpha$  precipitates deformation through twinning under higher local stress due to the dislocation pile-up at  $\alpha/\beta$  interface. Coarse  $\alpha$  precipitates have a large area of semi-coherent  $\alpha/\beta$  interface may show easier slip transfer and twinning, leading to higher ductility. Small  $\alpha$  precipitates have shown more  $\alpha/\beta$  interfaces, which could impede the

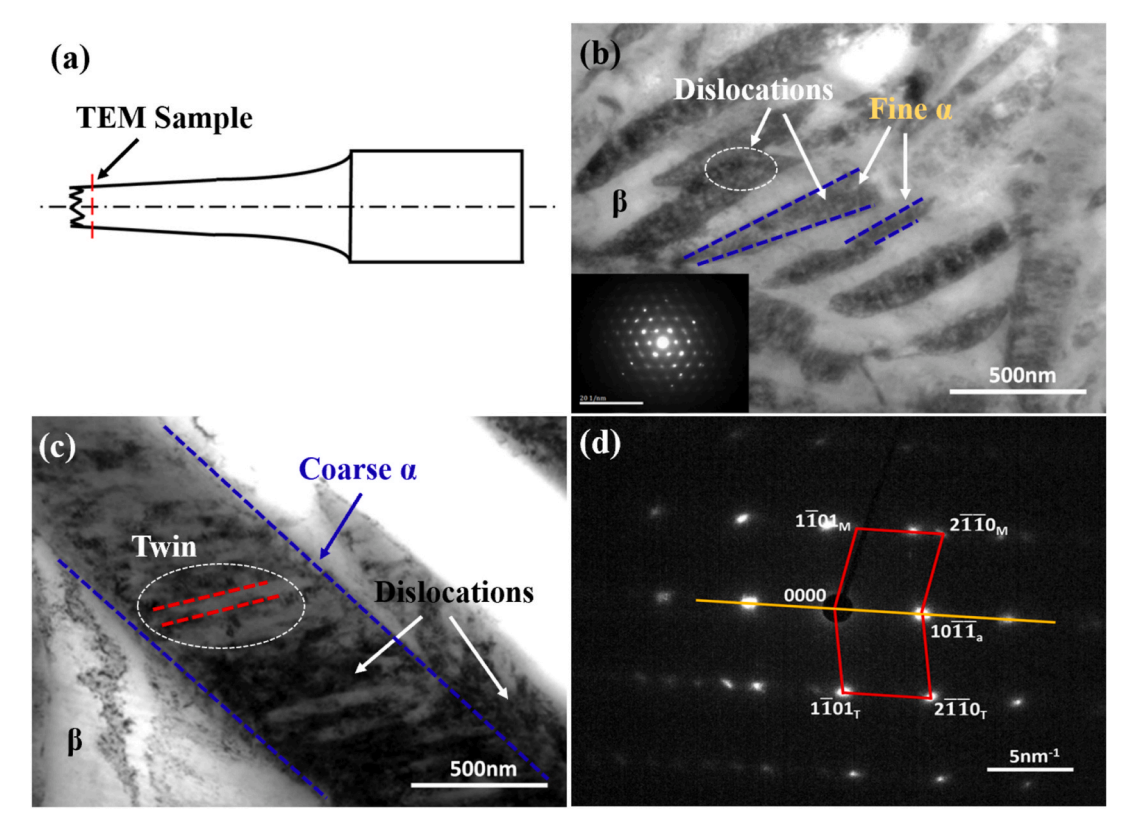


Fig. 5. Deformation microstructure characterization after the tensile test for samples with two-step aging at 700 °C/3h + 600 °C/3h: (a) Schematic drawing to indicate the location for TEM observation (red line), (b) a typical microstructure from the fine  $\alpha$  precipitate regions and selected area diffraction pattern, (c) a typical microstructure from the coarse  $\alpha$  precipitate regions and (d) selected area diffraction pattern showing deformation twins. (For interpretation of the references to color in this figure legend, the reader is referred to the Web version of this article.)

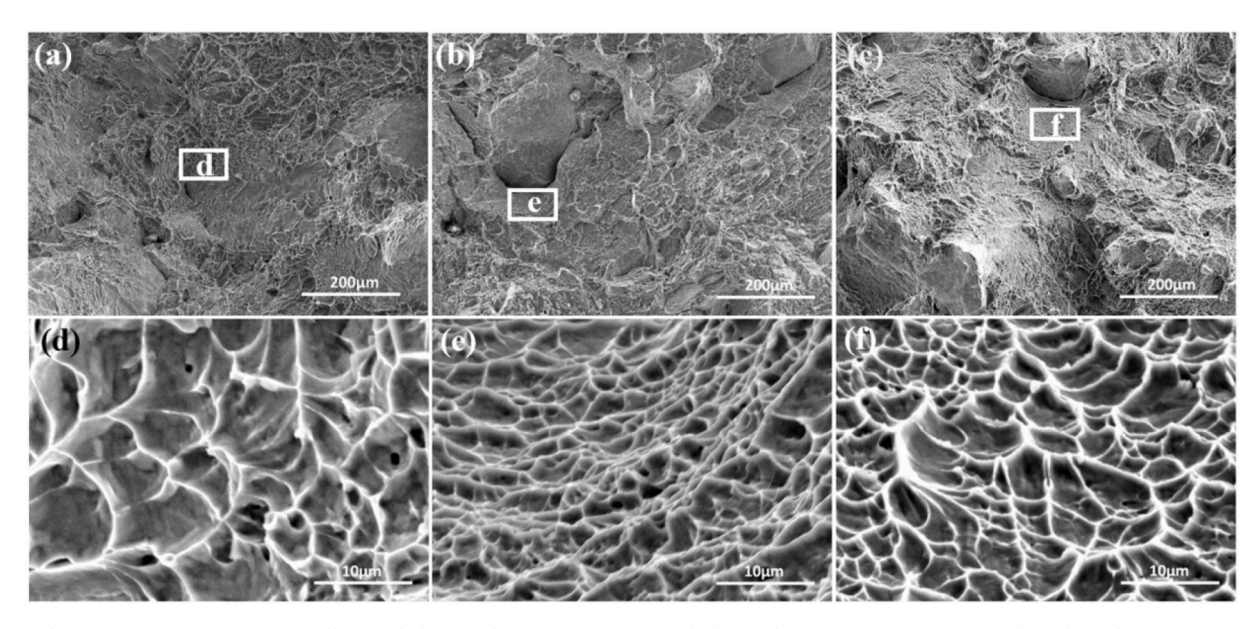


Fig. 6. Tensile fracture surfaces of Ti-55531 alloys with different heat treatments. (a) and (d) Tensile fracture surfaces of a sample with single-step aging at 700 °C/3 h, (b) and (e) tensile fracture surfaces of a sample with single-step aging at 700 °C/3 h, (c) and (f) tensile fracture surfaces of a sample with single-step aging at 700 °C/3 h + 600 °C/3 h.

dislocation motion and increase the strength. Coarse  $\alpha$  precipitates could sustain more deformation twin, leading to the accommodation of a much larger amount of strain in  $\alpha$ . Fine  $\alpha$  precipitates could get saturated (with dislocation density or twin) at lower macro-strain level, leading to strain incompatibility and the formation of nano voids [29].

Furthermore, the tensile fracture surface of Ti-55531 with different

heat treatments is shown in Fig. 6. All samples show a mixture of tensile failure mode including dimple zone and shear lip. Fig. 6 (a) and Fig. 6 (b) show the tensile fracture surfaces of samples with single-step aging at 700 °C/3 h and 600 °C/3h respectively. The enlarged image in Fig. 6 (d) and Fig. 6 (e) have shown uniformly-distributed dimples with similar sizes. Fig. 6(c) and (f) show the tensile fracture surface of the sample

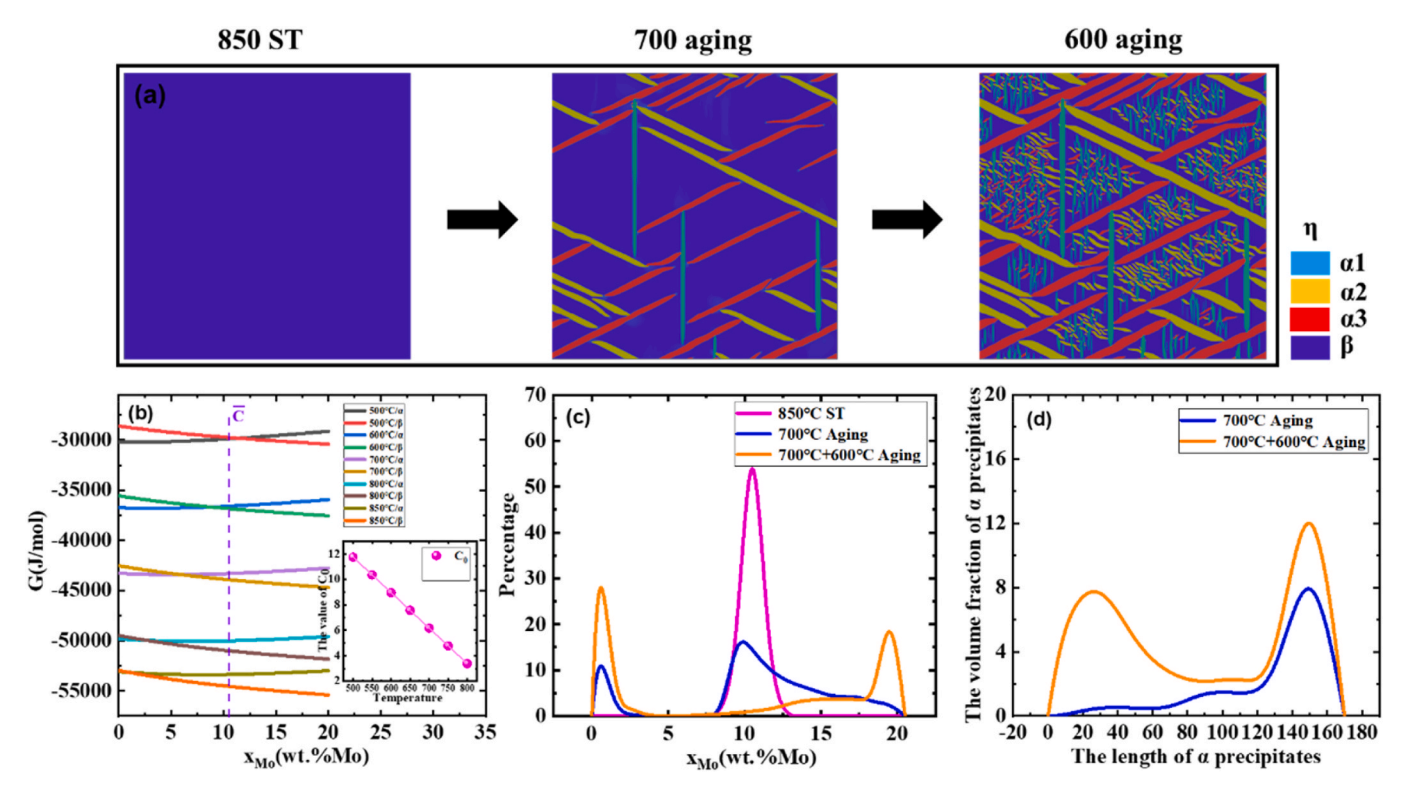


Fig. 7. Calculated microstructure and related analysis for two step-aging for Ti-Mo binary systems. (a) Microstructure for 850 °C solution treatment, followed by aging at 700 °C and 600 °C. (b) Free energy curves for  $\alpha$  and  $\beta$  phases at different temperatures from Pandat database. (c) Mo concentration distribution for the two-step aging process. (d) Length distribution of  $\alpha$  precipitates after aging at 700 °C and aging at 700 °C.

with two-step aging at 700 °C/3h + 600 °C/3h, which exhibits dimples of different sizes. The diameter of the dimple is consistent with the size of  $\alpha$  phase formed at different heat treatments and decides the ductility.

#### 4. Discussion

To describe the formation of bimodal  $\alpha$  precipitates in  $\beta$ -Ti alloys, phase field simulations considering Ti-10.5Mo (wt. %) have been proposed. Fig. 7(a) shows the microstructure evolution for 850 °C solution treatment (ST), followed by aging at 700 °C and 600 °C, respectively. The system shows pure  $\beta$  phase (dark blue) after ST, and coarse  $\alpha$  precipitates after aging at 700  $^{\circ}\text{C}\text{,}$  and a mixture of both coarse and fine  $\alpha$ precipitates after continuing aging at 600  $^{\circ}\text{C}.$  Our calculations are consistent with experimental observations. Further analysis for the free energy curves for  $\alpha$  and  $\beta$  phases at different temperatures in Fig. 7 (b) shows a linear temperature dependence of the intersection point  $c_0$ . The decrease of concentration difference  $\triangle c$  ( $c_{av}$ - $c_0$ ) between  $c_0$  and average concentration cav decides the change of nucleation mechanisms from conventional nucleation and growth at high aging temperature to pseudospinodal decomposition at low temperature [25]. Fig. 7(c) shows the concentration distribution for this two-step aging process. The system exhibits unimodal distribution with an average of 10.5 wt. % due to thermal fluctuation at 850 °C ST, bimodal distribution with relative low Mo concentration (~10 wt. %) in β-matrix after aging at 700 °C and relative high Mo concentration ( $\sim$ 19.5 wt. %) in  $\beta$ -matrix after aging at 700 °C + 600 °C. The Mo concentration ( $\sim$ 0.5 wt. %) in  $\alpha$  precipitates is fixed and the percentage increase. Fig. 7(d) shows the length distribution of  $\alpha$  precipitates after aging at 700 °C and aging at 700 °C + 600 °C, respectively. The system shows an obvious increase of fine  $\alpha$  precipitates and a weak increase of coarse  $\alpha$  precipitates, leading to the bimodal distribution. The coarse  $\alpha$  precipitates grow and fine  $\alpha$  precipitates nucleate at free space after 2nd aging at 600 °C.

The strength of near  $\beta$ -Ti alloys with fixed composition depends mainly on aging and thermomechanical processing by altering the

number density and distribution of  $\alpha$  precipitates. The effect of multiscale  $\alpha$  on the critical resolved shear stress (CRSS) can be empirically written as [30,31]:  $\tau^\kappa = \tau^\kappa_{\rm coarse} + \tau^\kappa_{\rm fine}$ , where  $\tau$  is the overall CRSS,  $\tau^\kappa_{\rm coarse}$  and  $\tau^\kappa_{\rm fine}$  are the contributions from the coarse and fine  $\alpha$  precipitates, respectively, and  $\kappa$  is the parameter for superposition. The critical resolved shear stress (CRSS) is inversely proportional to the inter-particle spacing and the yield strength can be written as:  $\sigma_y = \frac{K_{\rm coarse}}{L_{\rm coarse}} + \frac{K_{\rm fine}}{L_{\rm fine}} \sigma_y = \frac{K_{\rm coarse}}{L_{\rm coarse}} + \frac{K_{\rm fine}}{L_{\rm fine}}$ , where  $K_{\rm coarse}$  and  $K_{\rm fine}$  are the Taylor factor of coarse and fine  $\alpha$  precipitates, respectively, related to the CRSS;  $l_{\rm coarse}$  and  $l_{\rm fine}$  are the inter-particle spacing of coarse and fine  $\alpha$  precipitates, respectively, which are inversely proportional to the count densities. Thus, the relatively higher number density of hybrid  $\alpha$  microstructure (1.89 laths/ $\mu$ m²) after two-step aging could contribute to a higher strength than that of coarse  $\alpha$  microstructure (0.27 laths/ $\mu$ m²).

The appearance of twinning mechanisms in plasticity is frequently associated with a lack of ductility when these twins are generated by the accumulation of stacking faults on successive planes, and extend across the entire width of the grains [32]. However, when the system could deform by both glide of dislocations and mechanical twinning simultaneously, the materials have shown outstanding mechanical properties combining high strength and ductility, e.g., Twinning-Induced Plasticity (TWIP) steel [33] and titanium alloy [34]. The deformation mode of  $\alpha$ phase in near  $\beta$ -Ti alloys is either mechanical twinning [35,36], while the deformation mode of the  $\beta$  phase is stress-induced martensitic transformation [37–41]. It is worth noting that some  $\alpha$  laths can be deformed by slip [29], which are also found in Fig. 5. The  $\alpha/\beta$  interfaces influence the slip transmission and the deformation behaviors [42]. Both coarse  $\alpha$  and fine-scale  $\alpha$  precipitates contribute to the ductility of two step-aged samples through dislocation slip and deformation twinning. Thus, the deformation process for the bimodal  $\alpha$  microstructure produced by two-step aging can be summarized as a simple mixture of coarse and fine  $\alpha$ : i.e., fine-scale  $\alpha$  with high number density shows higher strength and coarse  $\alpha$  contributes to the high plasticity through

inducing both deformation twin and dislocation slip. Despite these findings, further in-situ observation of the deformation process is needed to confirm the deformation mechanism in future work.

#### 5. Conclusions

In summary, we designed a bimodal lamellar  $\alpha$  microstructure in Ti-55531 consisting of coarse and fine  $\alpha$  laths by a simple two-step aging heat treatment, which exhibits a superior combination of strength ( $\sim\!1.1$  GPa) and ductility ( $\sim\!19.5\%$ ). TEM observations and analysis have shown that the improved mechanical properties may be related to the high density of fine  $\alpha$  precipitates, and the activation of both twinning-induced plasticity and dislocation plasticity in the coarse  $\alpha$  precipitates. This work may shed light on the design of novel Ti-alloys with multimodal microstructures having enhanced comprehensive mechanical properties by simple multi-step aging.

#### Data availability

The raw/processed data required to reproduce these findings cannot be shared at this time due to technical or time limitations.

#### CRediT authorship contribution statement

Yalong Wang: Methodology, Visualization, Writing – original draft. Mengyuan Hao: Software, Formal analysis. Dian Li: Visualization, Writing – review & editing. Pei Li: Methodology, Resources. Qianglong Liang: Validation, Visualization. Dong Wang: Conceptualization, Supervision, Writing – review & editing. Yufeng Zheng: Visualization, Writing – review & editing. Qiaoyan Sun: Conceptualization, Methodology. Yunzhi Wang: Investigation, Writing – review & editing.

#### Declaration of competing interest

The authors declare that they have no known competing financial interests or personal relationships that could have appeared to influence the work reported in this paper.

#### Acknowledgments

Y. Wang, M. Hao, and D. Wang would like to acknowledge the support from the National Natural Science Foundation of China (Grants No. 52171012 and 51931004), Project supported by State Key Laboratory of Powder Metallurgy of Central South University, the National Key Research and Development Program of China (Grant No. 2016YFB0701302). D. Li and Y. Zheng appreciate the financial support by the faculty startup funding from University of Nevada, Reno. Y. Wang would like to acknowledge the support from the U.S. National Science Foundation under grant number DMR-1923929.

#### References

- D. Banerjee, J.C. Williams, Perspectives on titanium science and technology, Acta Mater. 61 (2013) 844–879.
- [2] R.R. Boyer, R.D. Briggs, The use of  $\beta$  titanium alloys in the aerospace industry, J. Mater. Eng. Perform. 14 (2005) 681–685.
- [3] D. Banerjee, J.C. Williams, Perspectives on titanium science and technology, Acta Mater. 61 (3) (2013) 844–879.
- [4] A. Ghosh, S. Sivaprasad, A. Bhattacharjee, S.K. Kar, Microstructure–fracture toughness correlation in an aircraft structural component alloy Ti–5Al–5V–5Mo–3Cr, Mater. Sci. Eng. A 568 (2013) 61–67.
- [5] M. Ahmed, D.G. Savvakin, O.M. Ivasishin, E.V. Pereloma, The effect of ageing on microstructure and mechanical properties of powder Ti–5Al–5Mo–5V–1Cr–1Fe alloy, Mater. Sci. Eng. A 605 (2014) 89–97.
- [6] K. Lu, The future of metals, Science 328 (2010) 319–320.
- [7] B.Z. Jiang, S. Emura, K. Tsuchiya, Microstructural evolution and its effect on the mechanical behavior of Ti-5Al-5Mo-5V-3Cr alloy during aging, Mater. Sci. Eng. A 731 (2018) 239–248.

- [8] L. Ren, W. Xiao, W. Han, C. Ma, L. Zhou, Influence of duplex ageing on secondary  $\alpha$  precipitates and mechanical properties of the near  $\beta$ -Ti alloy Ti-55531, Mater. Char. 144 (2018) 1–8.
- [9] H. Deng, L. Chen, W. Qiu, Z. Zheng, Y. Tang, Z. Hu, Y. Wei, Z. Xia, G. Le, J. Tang, X. Cui, Microstructure and mechanical properties of as-deposited and heat treated Ti–5Al–5Mo–5V–3Cr–1Zr (Ti-55531) alloy fabricated by laser melting deposition, J. Alloys Compd. 810 (2019), 151792.
- [10] R.P. Kolli, A. Devaraj, A review of metastable beta titanium alloys, Metals 8 (2018).
- [11] D. Qin, Y. Lu, Q. Liu, L. Zheng, L. Zhou, Transgranular shearing introduced brittlement of Ti–5Al–5V–5Mo–3Cr alloy with full lamellar structure at room temperature, Mater. Sci. Eng. A 572 (2013) 19–24.
- [12] C. Huang, Y. Zhao, S. Xin, W. Zhou, Q. Li, W. Zeng, Effect of microstructure on tensile properties of Ti–5Al–5Mo–5V–3Cr–1Zr alloy, J. Alloys Compd. 693 (2017) 582–591.
- [13] B. Jiang, S. Emura, K. Tsuchiya, Improvement of ductility in Ti-5Al-5Mo-5V-3Cr alloy by network-like precipitation of blocky α phase, Mater. Sci. Eng. A 722 (2018) 129–135.
- [14] Y. Wang, M. Chen, F. Zhou, E. Ma, High tensile ductility in a nanostructured metal, Nature 419 (2002) 912–915.
- [15] T.H. Fang, W.L. Li, N.R. Tao, K. Lu, Revealing extraordinary intrinsic tensile plasticity in gradient nano-grained copper, Science 331 (2011) 1587–1590.
- [16] A. Dehghan-Manshadi, R.J. Dippenaar, Development of α-phase morphologies during low temperature isothermal heat treatment of a Ti–5Al–5Mo–5V–3Cr alloy, Mater. Sci. Eng. A 528 (2011) 1833–1839.
- [17] C. Li, X. Wu, J.H. Chen, S. van der Zwaag, Influence of α morphology and volume fraction on the stress-induced martensitic transformation in Ti–10V–2Fe–3Al, Mater. Sci. Eng. A 528 (2011) 5854–5860.
- [18] Y. Ni, A.G. Khachaturyan, From chessboard tweed to chessboard nanowire structure during pseudospinodal decomposition, Nat. Mater. 8 (2009) 410–414.
- [19] S. Nag, Y. Zheng, R.E.A. Williams, A. Devaraj, A. Boyne, Y. Wang, P.C. Collins, G. B. Viswanathan, J.S. Tiley, B.C. Muddle, R. Banerjee, H.L. Fraser, Non-classical homogeneous precipitation mediated by compositional fluctuations in titanium alloys, Acta Mater. 60 (2012) 6247–6256.
- [20] Y. Zheng, R.E.A. Williams, J.M. Sosa, T. Alam, Y. Wang, R. Banerjee, H.L. Fraser, The indirect influence of the ω phase on the degree of refinement of distributions of the α phase in metastable β-Titanium alloys. Acta Mater. 103 (2016) 165–173.
- [21] D. Qin, Y. Lu, D. Guo, L. Zheng, Q. Liu, L. Zhou, Tensile deformation and fracture of Ti-5Al-5V-5Mo-3Cr-1.5Zr-0.5Fe alloy at room temperature, Mater. Sci. Eng. A 587 (2013) 100-109.
- [22] A. Boyne, D. Wang, R.P. Shi, Y. Zheng, A. Behera, S. Nag, J.S. Tiley, H.L. Fraser, R. Banerjee, Y. Wang, Pseudospinodal mechanism for fine  $\alpha/\beta$  microstructures in  $\beta$ -Ti alloys, Acta Mater. 64 (2014) 188–197.
- [23] H.J. Kong, T. Yang, R. Chen, S.Q. Yue, T.L. Zhang, B.X. Cao, C. Wang, W.H. Liu, J. H. Luan, Z.B. Jiao, B.W. Zhou, L.G. Meng, A. Wang, C.T. Liu, Breaking the strength-ductility paradox in advanced nanostructured Fe-based alloys through combined Cu and Mn additions, Scripta Mater. 186 (2020) 213–218.
- [24] X.Y. Li, L. Lu, J.G. Li, X. Zhang, H.J. Gao, Mechanical properties and deformation mechanisms of gradient nanostructured metals and alloys, Nat. Rev. Mater. 5 (2020) 706–723.
- [25] M.Y. Hao, Y.L. Wang, P. Li, T.L. Zhang, J.M. Zhu, D. Wang, Heterogeneous microstructure enhanced comprehensive mechanical properties in titanium alloys, JOM (J. Occup. Med.) 73 (2021) 3082–3091.
- [26] T. Zhang, D. Wang, J. Zhu, H. Xiao, C.T. Liu, Y. Wang, Non-conventional transformation pathways and ultrafine lamellar structures in γ-TiAl alloys, Acta Mater. 189 (2020) 25–34.
- [27] D. Gloaguen, G. Oum, V. Legrand, J. Fajoui, S. Branchu, Experimental and theoretical studies of intergranular strain in an alpha titanium alloy during plastic deformation, Acta Mater. 61 (2013) 5779–5790.
- [28] H.J. Li, W.P. Cai, Understanding the deformation mechanism of individual phases of a dual-phase beta type titanium alloy using in situ diffraction method, Mater. Sci. Eng. A 728 (2018) 151–156.
- [29] M. Sen, S. Suman, T. Banerjee, A. Bhattacharjee, S.K. Kar, Tensile deformation mechanism and failure mode of different microstructures in Ti-5AL-5Mo-5V-3Cr alloy, Mater. Sci. Eng. A 753 (2019) 156–167.
- [30] W.G. Zhu, Q.Y. Sun, C.S. Tan, P. Li, L. Xiao, J. Sun, Tensile brittleness and ductility improvement in a novel metastable beta titanium alloy with lamella structure, J. Alloys Compd. 827 (2020), 154311.
- [31] A. Devaraj, V.V. Joshi, A. Srivastava, S. Manandhar, V. Moxson, V.A. Duz, C. Lavender, A low-cost hierarchical nanostructured beta-titanium alloy with high strength, Nat. Commun. 7 (2016), 11176.
- [32] L.P. Kubin, B. Lisiecki, P. Caron, Octahedral slip instabilities in  $\gamma/\gamma$  superalloy single crystals CMSX-2 and AM3, Philos. Mag. A 71 (1995) 991–1009.
- [33] B.C. De Cooman, Y. Estrin, S.K. Kim, Twinning-induced plasticity (TWIP) steels, Acta Mater. 142 (2018) 283–362.
- [34] F. Sun, J.Y. Zhang, M. Marteleur, T. Gloriant, P. Vermaut, D. Laille, P. Castany, C. Curfs, P.J. Jacques, F. Prima, Investigation of early stage deformation mechanisms in a metastable beta titanium alloy showing combined twinning-induced plasticity and transformation-induced plasticity effects, Acta Mater. 61 (2013) 6406–6417.
- [35] M. Marteleur, F. Sun, T. Gloriant, P. Vermaut, P.J. Jacques, F. Prima, On the design of new β-metastable titanium alloys with improved work hardening rate thanks to simultaneous TRIP and TWIP effects, Scripta Mater. 66 (2012) 749–752.
- [36] X. Min, X. Chen, S. Emura, K. Tsuchiya, Mechanism of twinning-induced plasticity in  $\beta$ -type Ti–15Mo alloy, Scripta Mater. 69 (2013) 393–396.

- [37] E. Bertrand, P. Castany, I. Péron, T. Gloriant, Twinning system selection in a metastable β-titanium alloy by Schmid factor analysis, Scripta Mater. 64 (2011) 1110–1113.
- [38] X. Min, S. Emura, X. Chen, X. Zhou, K. Tsuzaki, K. Tsuchiya, Deformation microstructural evolution and strain hardening of differently oriented grains in twinning-induced plasticity  $\beta$  titanium alloy, Mater. Sci. Eng. A 659 (2016) 1–11.
- [39] J. Zhang, C.C. Tasan, M.J. Lai, A.C. Dippel, D. Raabe, Complexion-mediated martensitic phase transformation in Titanium, Nat. Commun. 8 (2017), 14210.
- [40] Q. Liang, Z. Kloenne, Y. Zheng, D. Wang, S. Antonov, Y. Gao, Y. Hao, R. Yang, Y. Wang, H.L. Fraser, The role of nano-scaled structural non-uniformities on deformation twinning and stress-induced transformation in a cold rolled multifunctional  $\beta$ -titanium alloy, Scripta Mater. 177 (2020) 181–185.
- [41] G.H. Zhao, X. Xu, D. Dye, P.E.J. Rivera-Diaz-del-Castillo, Microstructural evolution and strain-hardening in TWIP Ti alloys, Acta Mater. 183 (2020) 155–164.
- [42] P. Zhao, C. Shen, M.F. Savage, J. Li, S.R. Niezgoda, M.J. Mills, Y. Wang, Slip transmission assisted by Shockley partials acrossα/βinterfaces in Ti-alloys, Acta Mater. 171 (2019) 291–305.